Observation of acoustic Floquet π modes in a time-varying lattice

Zhao-xian Chen [1,2,*], An Chen [1,*], Yu-Gui Peng,[3] Zheng-wei Li,[1] Bin Liang,[1,†] Jing Yang,[1,‡] Xue-Feng Zhu [3,§]
Yan-qing Lu [2] and Jian-chun Cheng[1,‖]

[1]*Collaborative Innovation Center of Advanced Microstructures and Key Laboratory of Modern Acoustics, MOE, Institute of Acoustics, Department of Physics, Nanjing University, Nanjing 210093, People's Republic of China*

[2]*College of Engineering and Applied Sciences, Nanjing University, Nanjing 210093, People's Republic of China*

[3]*School of Physics and Innovation Institute, Huazhong University of Science and Technology, Wuhan, Hubei 430074, People's Republic of China*

Time modulation provides an important degree of freedom for classical wave steering in topological manners. Rather than using the spatial dimension to mimic time, here we design and implement an acoustic temporal lattice with time-varying couplings to demonstrate a unique type of strongly localized Floquet π modes that are gauge independent and can be robustly excited at the frequency in the nontrivial band gap. We observe the topological phase transitions by changing modulation frequency, consistent with the calculated quasienergy spectra. Our work paves the way for investigating intrinsic characteristics of various temporal systems and may inspire other intriguing discoveries in topological systems, such as higher-order temporal Floquet topological insulators.

Introduction. In recent years, time modulation has been attracting surging attention as it provides more degrees of freedom for wave manipulations [1–5]. Generally speaking, time modulation includes nonperiodic operation and abrupt temporal switching, which reshape the paradigm for time reversal acoustics [6,7], broadband impedance matching and absorption [8–10], temporal antireflecting coating [11], non-Hermitian response [12,13], and so on. However, periodic time modulation always plays a central role and can be analyzed with the well-established Floquet theorem. One appealing application for periodic modulations in time is to make the magnet-free nonreciprocal devices or multifunctional metasurfaces by designing asymmetric mode transitions in k-ω space [14–17]. Meanwhile, periodic time modulation has been proposed as an essential strategy to tailor the topological phases, which brings new insights for classical wave steering [18–21]. Specifically, by applying judiciously designed time modulation, the classical wave systems can behave as Floquet topological insulators (FTIs) to support localized edge states [22–33].

However, FTIs need the hopping or on-site energy modulation with time, making its realization very challenging. Alternatively, researchers mainly focus on waveguide platforms for classical wave manipulation, where the governing paraxial wave equation takes a similar form to the time-dependent Schrödinger equation, and the propagating axis in space dimension can serve as the synthetical time dimension.

Although the waveguide systems also have the potential for studying the topological pumping and adiabatic processes [34–40], they are static in nature and usually unconfigurable. As a result, the localized robust edge modes in such time-independent FTIs are intrinsically reciprocal. In addition, the spatial modulation in waveguide systems does not bring a real frequency band gap, and the wave energy of the Floquet π mode oscillates between the coupled waveguides along the propagating direction, making it gauge dependent. For example, the Floquet π modes can only be conditionally excited by well matching the source with the instantaneous modal profile at the initial position [29].

To break through these limitations in static waveguide systems, we propose a time-varying Su-Schrieffer-Heeger (SSH) model and experimentally implement it in a one-dimensional (1D) acoustic cavity lattice with the adoption of an electric-circuit-driven dynamic coupling strategy. Under moderate modulation frequencies, we univocally excite the localized edge modes, which are Floquet π modes as they emerge at half the driving frequency. Distinctive from their counterparts in static waveguide systems, the Floquet π modes in our system with real-time modulation are hybridizations of adjacent Floquet harmonics in real frequency band gaps. Thus, the Floquet π modes can be stably excited by choosing the frequencies in the π gaps. Taking advantage of the Floquet theory, we calculate the quasienergy bands of the systems to elaborate on the band degeneracy mechanism and related topological phase transition. For comparison, we experimentally demonstrate that the π modes are absent when the system is in both low- and high-modulation-frequency regimes. To our knowledge, the temporal lattice is utilized for the first time to demonstrate the Floquet π modes, which may inspire other topological discoveries for time-dependent wave systems.

―――――――

*These authors contributed equally to this work.

†Corresponding author: liangbin@nju.edu.cn

‡Corresponding author: yangj@nju.edu.cn

§Corresponding author: xfzhu@hust.edu.cn
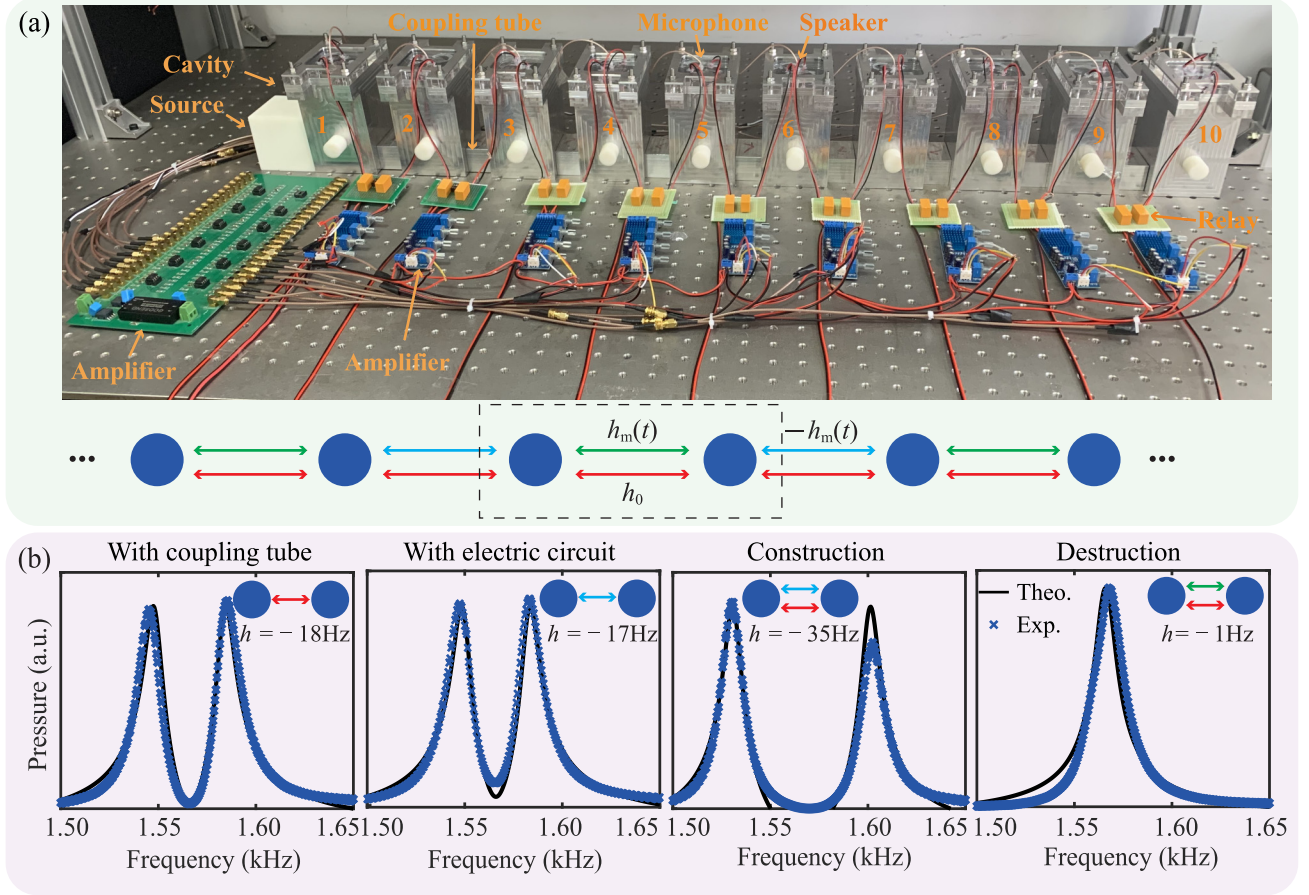
‖Corresponding author: jccheng@nju.edu.cn

FIG. 1. Acoustic implementation of the time-varying SSH model. (a) A photograph of the acoustic lattice with ten coupled cavities. The adjacent cavities are interlinked with both the air tubes (for static coupling h_0) and the electric setups [for dynamic coupling $h_m(t)$], which have microphones, amplifiers, DPDT relays, and loudspeakers. The lower panel shows the tight-binding model for the generalized time-dependent SSH model, with the dashed box representing a unit cell. (b) Experimentally measured (crosses) and theoretically calculated (solid curves) pressure amplitudes in the excited cavity under different coupling conditions.

Acoustic realization of time-dependent SSH model. To excite the robust Floquet π mode in the time domain, we design and fabricate a temporal 1D acoustic lattice with time-modulated couplings, mimicking a generalized time-varying SSH model [41–43]. As shown in Fig. 1(a), the acoustic lattice consists of 10 identical metallic and cuboid cavities labeled from 1 to 10. The cavities of height 10 cm support the first-order resonance at $\omega_0/2\pi = 1568$ Hz with dipole like modal profiles. With a proper arrangement of static coupling tubes, both positive and negative couplings can readily be obtained between these cavities [44–46]. Here we link the cavities at the bottom with straight tubes, contributing a static coupling h_0 [47]. In addition, adjacent cavities are mutually connected with the dynamic coupling generated by designed feedback circuits, which consist of microphones (for input), signal amplifiers (with direct current power supplies), and loudspeakers (for output). Taking two cavities labeled n and $n + 1$ for example, the sound is detected at cavity n ($n + 1$) by the microphone and then coupled to $n + 1$ (n) by using the speaker after amplification. Between the amplifiers and loudspeakers, there are double-pole, double-throw (DPDT) relays so that the electric connections (in-phase or out-of-phase) can modulate with the control signals [47]. As a result, the active

circuits provide a tunable coupling $h_m(t)$, which can work together with the static coupling h_0. By periodically controlling the relays and ignoring the higher-order Fourier components of $h_m(t)$, as shown in the lower panel of Fig. 1(a), our acoustic crystal mimics a generalized time-dependent SSH model with the staggered couplings,

$$
\mathbf{H}(t) = \sum_{n=1}^{N} (\omega_0 + i\gamma) c_n^\dagger c_n
$$
$$
+ \sum_{n=1}^{N-1} [h_0 + (-1)^n h_m \cos(\omega_m t)] c_n^\dagger c_{n+1} + \text{H.c.,} \quad (1)
$$

where n denotes the site indices, h_m is the effective modulation amplitude, ω_m is the modulation frequency, and $c_n^\dagger$ and c_n are the creation and annihilation operators for the nth site, respectively.

Before showcasing the Floquet π modes of this time-varying acoustic lattice in the time domain, we experimentally verified the effectiveness of this time-dependent coupling unit with a static two-resonator system, which can be described by a static Hamiltonian $\mathbf{H} = \begin{bmatrix} \omega_0 + i\gamma & h \\ h & \omega_0 + i\gamma \end{bmatrix}$, where γ is the intrinsic loss of cavities and h is the total coupling effect [48].
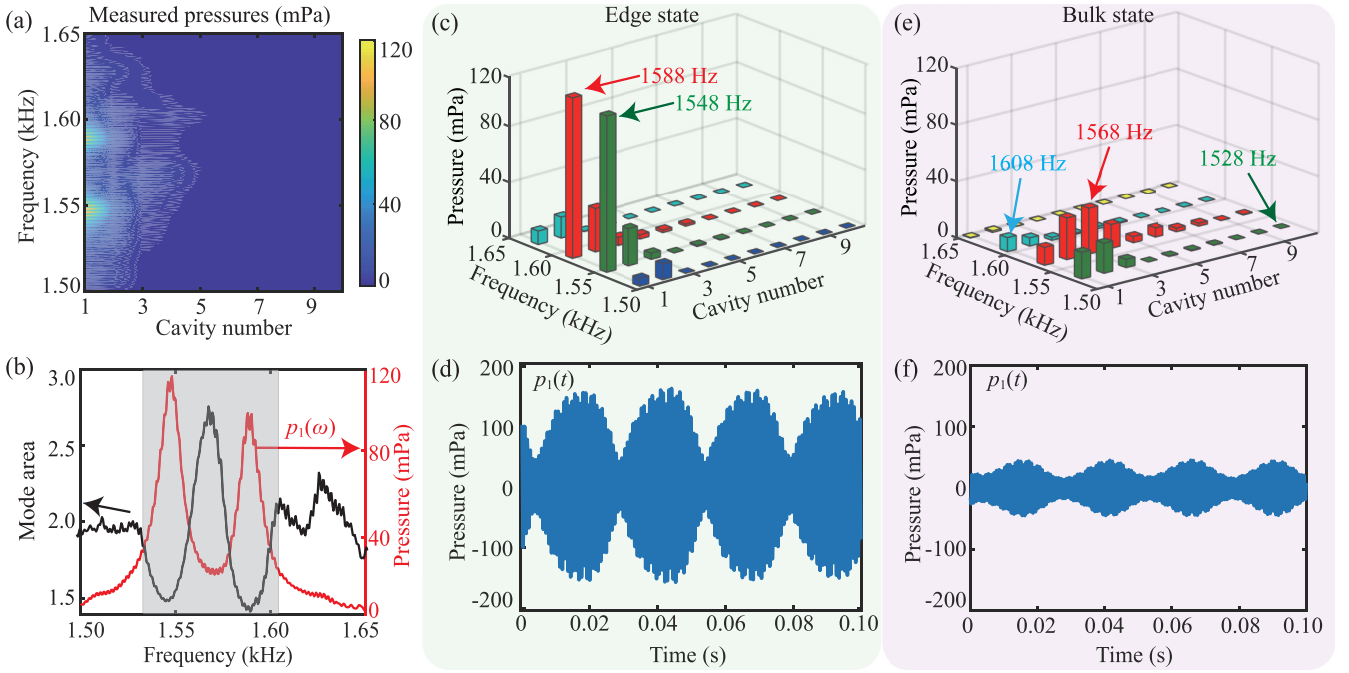
FIG. 2. Floquet π modes with $\omega_m/2\pi = 40$ Hz. (a) The measured pressure distributions in the lattice with the boundary excitation. (b) The pressure $p_1(\omega)$ and field area $S_{\text{field}}(\omega)$ with the dark region denoting the range of bulk states from $\omega_0 - 2h_0$ to $\omega_0 + 2h_0$. [(c) and (d)] Pressure distributions for the edge state with a single-frequency source at $\omega/2\pi = 1588$ Hz. $p_1(t)$ is the transient pressure in the first cavity. [(e) and (f)] Pressures for the bulk state with a sound source at $\omega/2\pi = \omega_0/2\pi = 1568$ Hz.

As shown in Fig. 1(b), by fitting the spectra of the excited cavity, we obtain the static coupling of $h_0/2\pi = -18$ Hz and the tunable coupling of $|h_m^{\text{static}}/2\pi| = 17$ Hz. The signs of couplings can be determined by the phase difference between the two cavities. When both couplings are present, the total coupling is $h/2\pi = -35$ Hz (or $h/2\pi = -1$ Hz) if they are with the same (or opposite) signs, demonstrating the linear superposition relation between them. Thus, when use square-wave voltage signals to control the relays, h_m^{static} periodically switches from positive to negative, becoming time modulated $h_m(t)$. Without changing the cavities' boundary conditions, such dynamic coupling has negligible effects on the system's chiral symmetry and can be modulated fast and freely without introducing any noise or dissipation, making our system a versatile platform for studying topological physics. In addition, the electric elements in the coupling circuits introduce negligible phase delays, and the mutual couplings here are real valued and are different from the previous experimental implementations with complex values [49,50].

Observation of floquet edge modes. We introduce time modulation to the acoustic lattice to study the dynamics of the Floquet π modes. By exciting the left-most cavity (labeled 1) with a swept-frequency signal, we measured the sound pressures of the system with modulation frequency $\omega_m/2\pi = 40$ Hz. Figure 2(a) shows that the pressures have two prominent peaks around 1548 and 1588 Hz, corresponding to the edge modes in the Floquet band gaps. To analyze the localization property of the modes, we define the excited field area as

$$S_{\text{field}}(\omega) = \frac{\sum |p_n(\omega)|}{\max\{|p_n(\omega)|\}}, \qquad (2)$$

where $p_n(\omega)$ is the pressure in the nth cavity. It is clear that a smaller S_{field} means a stronger localization. In Fig. 2(b), we display both $S_{\text{field}}(\omega)$ and $p_1(\omega)$ for comparison. The sound waves around $\omega_0 \pm \omega_m/2$ (here are 1588 and 1548 Hz) have the maximum pressures but correspond to the minimum field areas, demonstrating a strong localization of the edge modes. Though the Floquet bands are periodic, it should be noted that only these π modes within the bulk band range (the dark region from $\omega_0 - 2h_0$ to $\omega_0 + 2h_0$) can be effectively excited.

We switched to single-frequency signals for the excitation to further investigate these π modes. When we set $\omega/2\pi = 1588$ Hz, as shown in Fig. 2(c), the sound wave concentrates at the outmost cavity and is remarkably converted to 1548 Hz. In Fig. 2(d), the beat effect of transient pressure $p_1(t)$ also demonstrates that the edge modes are the hybridization of $\omega_0 \pm \omega_m/2$. We need to stress that the Floquet π modes are with specific frequencies in the Floquet band gaps, rendering more robustness for excitation. This is distinct from their counterparts in the static waveguide platform, where the space serves as the synthetical time dimension, and the Floquet π modes can only be excited by matching the source with the instantaneous modal profile as the frequency band gap is absent [29]. On the other hand, when we use $\omega = \omega_0$ as the working frequency, the bulk modes are excited. As shown in Figs. 2(e) and 2(f), the excited pressures are much smaller than the edge states. However, due to the dissipation of cavities, the excited bulk modes cannot spread throughout the whole lattice, which leads to the difference between the experimental and theoretical results in the Supplemental Sec. V [47].

Floquet phase transitions. To study the modulation frequency's effect on the Floquet π modes, we measured $p_1(\omega)$
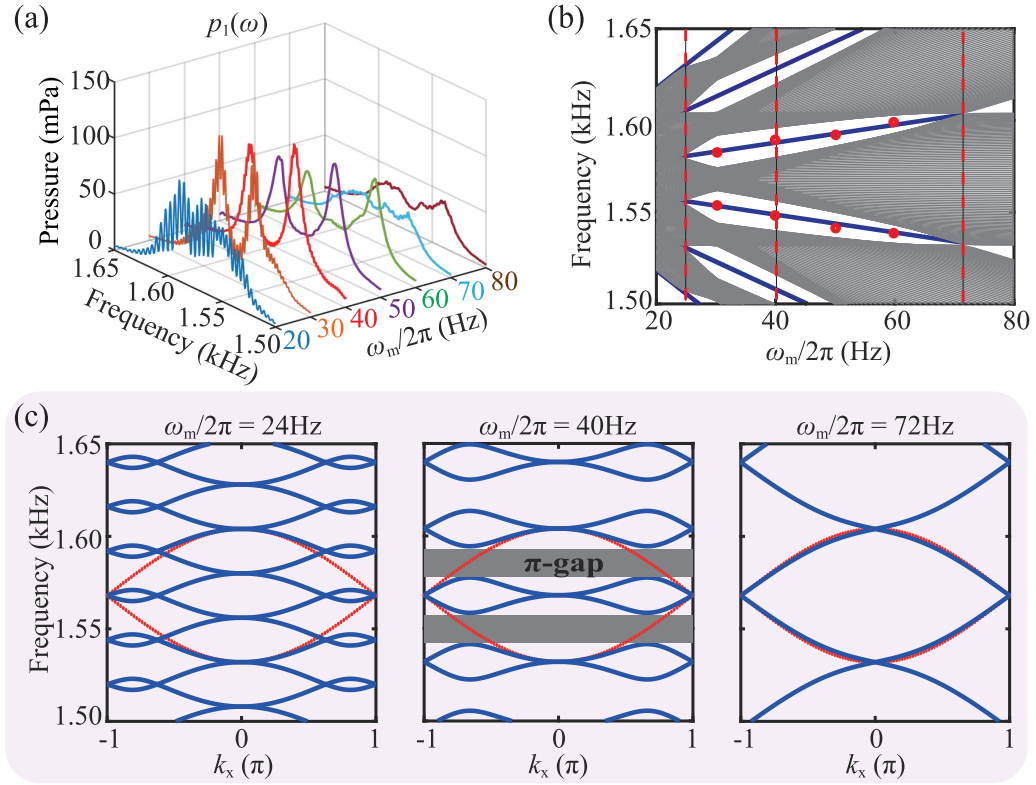
FIG. 3. Quasienergy spectra for the time-periodic SSH model. (a) Measured pressure $p_1(\omega)$ at different ω_m. (b) Quasienergies of the SSH model with opening boundary conditions. In the calculations, we set $N = 40$ and $h_m/2\pi = 10$ Hz. The gray regions denote the bulk band, and the blue curves indicate the edge modes in the π gaps. Red dots are the measured pressure peaks in (a). Red dashed curves denote three frequencies analyzed in (c). (c) Quasienergy bands (blue curves) of the time-periodic SSH model in the momentum space at different ω_m. Red curves are energy bands of the static SSH model with $h_m = 0$, and are used to guide the catch for the Floquet replicas. The gray regions in the middle column denote the π gaps.

with different ω_m. As shown in Fig. 3(a), by setting the sweeping step to be 10 Hz, only for ω_m within a particular range from 30 to 60 Hz, $p_1(\omega)$ has two prominent peaks, where the π modes are excited. To elaborate on the mechanism of π modes with time modulation, we utilize the Floquet theory to calculate the quasienergy of the time-periodic Hamiltonian (see Appendix A). In this case, the time-dependent model becomes a time-independent eigenvalue problem in the direct-product Floquet space: $\mathcal{H} \otimes \mathcal{T}$, where $\mathcal{H}$ is the conventional Hilbert space and $\mathcal{T}$ is the space of time-periodic functions spanned by $e^{ij\omega_m t}$, with j denoting the jth Floquet replica [42]. For the time-dependent SSH model with open boundaries in Eq. (1), we calculate the quasienergy as a function of ω_m. In Fig. 3(b), replicas for $j \in [-2, 2]$ are provided together with the measured pressure peaks (red dots) in Fig. 3(a) [47]. Because of the chiral symmetry, the quasienergy spectra are symmetric about 1568 Hz. It is evident that the Floquet π modes (blue curves) are only available within a particular ω_m range, which can be explained by the degeneracy of the Floquet replicas. When $\omega_m > 4h_0$, the modulation is so fast that the replicas do not overlap with each other, and the π gaps therein are trivial. At $\omega_m = 4h_0$ (here is 72 Hz), as shown by the right column in Fig. 3(c), the gaps are closed because the $j = 0$ band touches the adjacent replicas with $j = \pm 1$ at $\omega_0 \pm \omega_m/2$. By further decreasing ω_m, the overlap between

the $j = 0$ and ± 1 replicas opens the gaps again, which is given in the middle column of Fig. 3(c) with $\omega_m/2\pi = 40$ Hz. As a result, the closing and reopening process switches the π gaps at $\omega_0 \pm \omega_m/2$ from trivial to nontrivial, which can be proved by calculating the Zak phases [42]. When we continue to decrease the modulation frequency and set $\omega_m < 4h_0/3$, the modulation is so slow that more replicas overlap with each other, and new degeneracies appear within the spectral range of the $j = 0$ replica. However, as shown by the left column of Fig. 3(c), the driving-induced gaps become subtle and unnoticeable. We note that the phase transition points correspond to the cases where new degeneracies occur.

Wave dynamics for low- and high-frequency regimes. As has been explained, the Floquet π modes become unobservable (absent) when the system modulates in the low- (high-) frequency regimes since too many (no) Floquet replicas overlap. When the modulation goes to the low-frequency regime, more replicas overlap with each other, switching the topology from trivial to nontrivial and vice versa [51]. However, for the specific case with $\omega_m/2\pi = 20$ Hz, as shown in Fig. 4(a), there is no edge mode in the frequency range of $[\omega_0 - 2h_0, \omega_0 + 2h_0]$, where the pressure distributions become uniform. When we compare Fig. 4(c) with Fig. 4(d), the pressure distributions at the high modulation frequency of $\omega_m/2\pi = 80$ Hz are almost identical to those with no modulation, viz., $h_m = 0$. In other
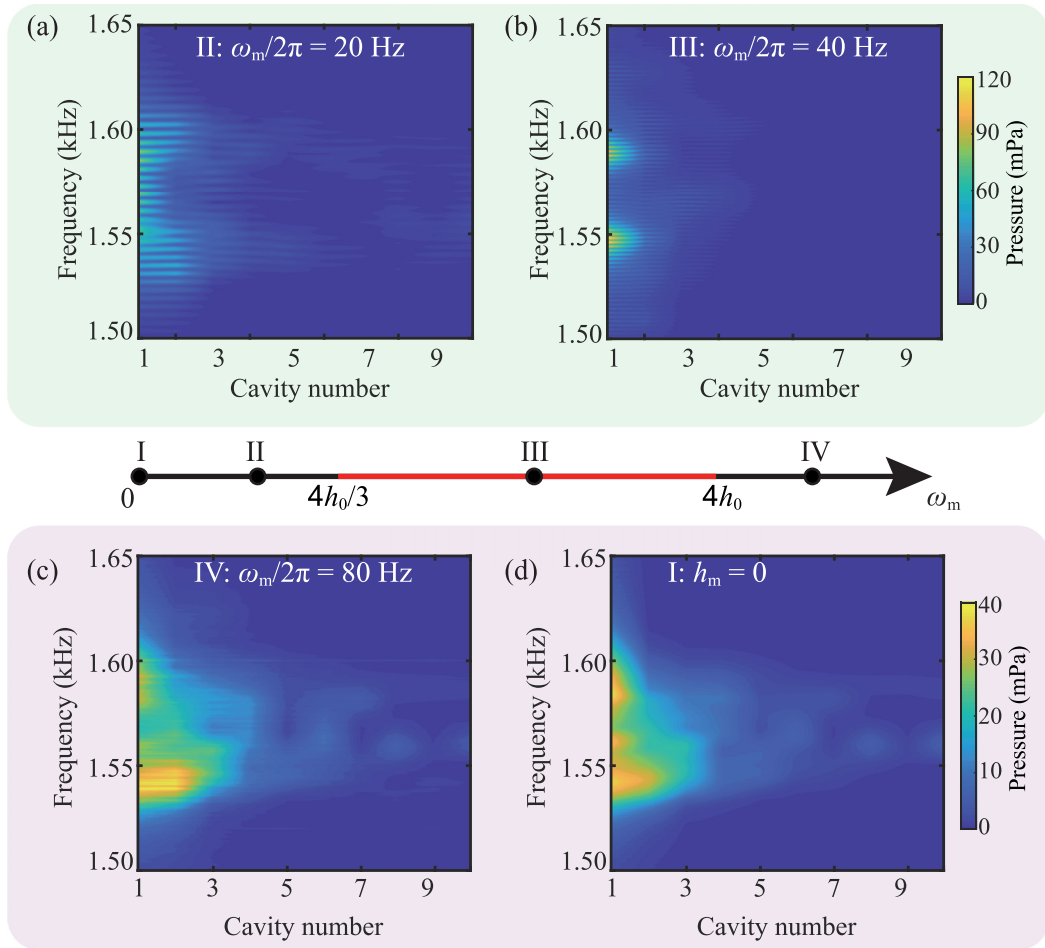
FIG. 4. Measured pressure distributions with different modulation conditions. [(a)–(c)] The time-varying cases with the modulation frequencies in the (a) low-, (b) moderate-, and (c) high-frequency regimes, respectively. (d) The static case without the time-varying couplings. All four cases are marked in the ω_m axis with the red region representing the moderate frequency range of $4h_0/3 < \omega_m < 4h_0$.

words, in the high-frequency regime, the modulation seems to "do nothing" because the replicas are separated from each other. We note that the sound wave propagates into the interior region, while the pressures at the boundary are much smaller than the π modes with $\omega_m/2\pi = 40$ Hz, as shown in Fig. 4(b) for comparison. In summary, we failed to observe the Floquet π mode in both the low- and high-frequency regimes, and the underlying reasons are distinct.

Conclusion. In this work, we have developed an elegant method to implement dynamic systems with real time-modulation and demonstrated the Floquet phase transitions in an acoustic temporal lattice. We realize a time-dependent SSH model in acoustics with staggered couplings controlled by electric relays. The nontrivial Floquet π modes in temporal lattices, distinctive from the counterparts in the static waveguide systems, are unambiguously excited in the experiments by choosing the correct excitation frequency in the band gap (see Appendix B for comparison). Resulting from time modulation and hybridization of adjacent Floquet replicas, the real band gap in frequency provides us with more degrees of freedom for robust edge state manipulation. Notably, by utilizing the electric circuits rather than physical

overlap, the dynamic coupling is favorable for extending the system into three or higher dimensions with the chiral symmetry protected. Our proposal not only opens the door of the real time-dependent Floquet systems for various significant applications, such as acoustic diodes and isolators, but also facilitates the realization of other intriguing matter, such as time crystals [52–54].

Appendix A: Floquet energy band. For the generalized SSH model with time-dependent couplings, we use the Floquet theory to deal with the time-periodic Hamiltonian $\mathbf{H}(t + 2\pi/\omega_m) = \mathbf{H}(t)$, where ω_m is the modulation frequency. The quasienergy band can be calculated by using the Floquet mode expansion method. According to this theory, the state function can be written as a superposition of Floquet states

$$|\mathbf{\Psi}(t)\rangle = e^{i\varepsilon t}|\boldsymbol{u}(t)\rangle, \tag{A1}$$

where ε is the quasienergy and $|\boldsymbol{u}(t)\rangle$ is the corresponding Floquet mode. Since the eigenvalues belong to an extended Hilbert space, the quasienergies are defined with integer multiplies of ω_m, and the Floquet modes are also periodic with $2\pi/\omega_m$. By taking Eq. (A1) into the Schrödinger-type wave equation, we obtain a new eigenvalue equation

$$\left(\mathbf{H}(t) + i\frac{d}{dt}\right)|\boldsymbol{u}(t)\rangle = \varepsilon|\boldsymbol{u}(t)\rangle. \tag{A2}$$

Using the spectral decomposition of the Hamiltonian and the Floquet modes, viz.,

$$\mathbf{H}(t) = \sum_{f=-\infty}^{\infty} e^{if\omega_m t}\mathbf{H}_f, \tag{A3a}$$

$$|\boldsymbol{u}(t)\rangle = \sum_{f=-\infty}^{\infty} e^{if\omega_m t}|u^f\rangle, \tag{A3b}$$

we can simplify the dynamic wave equation as a time-independent Floquet equation,

$$(\mathbf{H}_0 - f\omega\mathbf{I})|u^f\rangle + \sum_{m\neq 0}\mathbf{H}_m|u^{f-m}\rangle = \varepsilon|u^f\rangle, \tag{A4}$$

where f is an integer.

For the time-dependent SSH model in Eq. (1), its Hamiltonian can be treated as a sum of static and dynamic parts,

$$\mathbf{H}(t) = \mathbf{H}_0 + \mathbf{H}_t(t), \tag{A5}$$

where

$$\mathbf{H}_0 = \sum_{n=1}^{N}(\omega_0 + i\gamma)c_n^\dagger c_n + \sum_{n=1}^{N-1}h_0 c_n^\dagger c_{n+1} + \text{H.c.}, \tag{A6a}$$

$$\mathbf{H}_t(t) = \sum_{n=1}^{N-1}(-1)^n h_m \cos(\omega_m t)c_n^\dagger c_{n+1} + \text{H.c.}. \tag{A6b}$$

By reformulate the time-dependent Hamiltonian with an exponential function $\mathbf{H}_t(t) = \mathbf{H}_1 e^{i\omega_m t} + \mathbf{H}_{-1}e^{-i\omega_m t}$, all the Hamiltonian can be expressed by a $N \times N$ matrix,

$$\mathbf{H}_0 = \begin{pmatrix} i\gamma & h_0 & 0 & \\ h_0 & i\gamma & h_0 & \cdots \\ 0 & h_0 & i\gamma & \\ & \vdots & & \ddots \end{pmatrix}_{N\times N}, \tag{A7a}$$

$$\mathbf{H}_{\pm 1} = \frac{1}{2}\begin{pmatrix} 0 & -h_m & 0 & \\ -h_m & 0 & h_m & \cdots \\ 0 & h_m & 0 & \\ & \vdots & & \ddots \end{pmatrix}_{N\times N}. \tag{A7b}$$

Note here we set $\omega_0 = 0$ for a reference value. As a result, the eigenvalue equation can be represented with a block-matrix operator

$$\begin{pmatrix} \ddots & & & & \\ \mathbf{H}_1 & \mathbf{H}_0 - \omega_m\mathbf{I} & \mathbf{H}_{-1} & & \\ & \mathbf{H}_1 & \mathbf{H}_0 & \mathbf{H}_{-1} & \\ & & \mathbf{H}_1 & \mathbf{H}_0 + \omega_m\mathbf{I} & \mathbf{H}_{-1} \\ & & & & \ddots \end{pmatrix}\begin{pmatrix} \vdots \\ u^{-1} \\ u^0 \\ u^1 \\ \vdots \end{pmatrix}$$
$$= \varepsilon\begin{pmatrix} \vdots \\ u^{-1} \\ u^0 \\ u^1 \\ \vdots \end{pmatrix}. \tag{A8}$$

By truncating Eq. (A8) at a finite f, we can get the converged eigenvalues.

Appendix B: Comparison of the floquet edge modes. Table I summarizes the comparison of the Floquet π modes in static waveguide or time-varying cavity systems. Here $H(x)$ ($H(t)$) is the Hamiltonian of the waveguide section along the propagating direction x (the time-varying cavity system with time t), $|\Psi(x)\rangle$ ($|\Psi(t)\rangle$) is the wave function in the waveguides (cavities), and $|s(t)\rangle$ is the stably applied source. The distinction between the Floquet π modes in these two settings can also be seen in Fig. 5, which vividly presents the wave dynamics of the two edge modes.

TABLE I. Comparison of the Floquet π modes in the waveguide or time-varying systems.

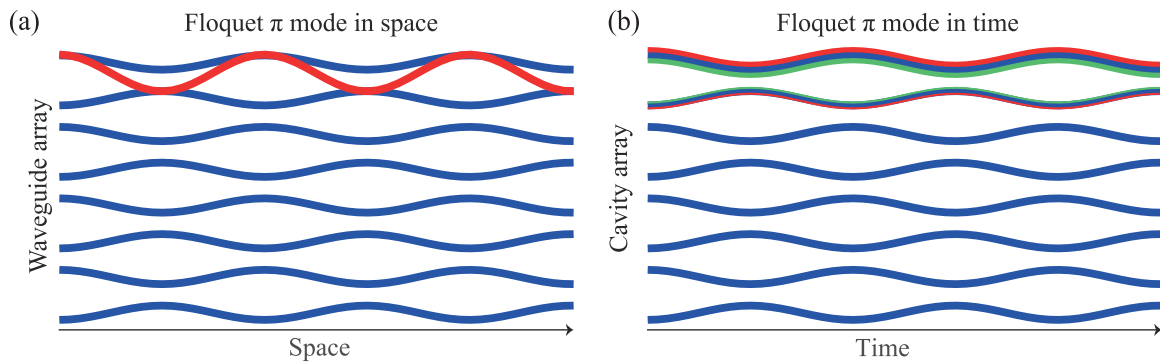|	Static waveguide system	Real time-varying system
Wave equation	$-i\frac{d}{dx}|\Psi(x)\rangle = H(x)|\Psi(x)\rangle$	$-i\frac{d}{dt}|\Psi(t)\rangle = H(t)|\Psi(t)\rangle + |s(t)\rangle$
On-site energy	Propagation constant	Resonant frequency
Frequency conversion	Absent	Yes
Source introduction	Initially introduced	Stably applied
Gauge-dependence	Yes	No

FIG. 5. Schematic of the Floquet π modes in the waveguide (a) or time-varying system (b). For the waveguide system, the edge mode energy, denoted by the red line, oscillates between the two outmost waveguides. Thus, the π mode is gauge dependent and can only be excited by matching the source with the initial modal profile. Contrarily, the π mode in the time-varying lattice is gauge independent and can be robustly excited by using the frequencies in the $\pm\pi$ gaps, denoted by the red and green lines.

[1] D. L. Sounas and A. Alù, Non-reciprocal photonics based on time modulation, Nat. Photon. **11**, 774 (2017).

[2] E. Galiffi, R. Tirole, S. Yin, H. Li, S. Vezzoli, P. A. Huidobro, M. G. Silveirinha, R. Sapienza, A. Alù, and J. B. Pendry, Photonics of time-varying media, Adv. Photon. **4**, 014002 (2022).

[3] F. Zangeneh-Nejad and R. Fleury, Active times for acoustic metamaterials, Rev. Phys. **4**, 100031 (2019).

[4] I. A. D. Williamson, M. Minkov, A. Dutt, J. Wang, A. Y. Song, and S. Fan, Integrated nonreciprocal photonic devices with dynamic modulation, Proc. IEEE **108**, 1759 (2020).

[5] C. Caloz and Z. L. Deck-Léger, Spacetime metamaterials—Part I: General concepts, IEEE Trans. Antenn. Propag. **68**, 1569 (2020).

[6] M. Fink, D. Cassereau, A. Derode, C. Prada, P. Roux, M. Tanter, J.-L. Thomas, and F. Wu, Time-reversed acoustics, Rep. Prog. Phys. **63**, 1933 (2000).

[7] M. Fink and C. Prada, Acoustic time-reversal mirrors, Inverse Probl. **17**, R1 (2001).

[8] A. Shlivinski and Y. Hadad, Beyond the Bode-Fano bound: Wideband impedance matching for short pulses using temporal switching of transmission-line parameters, Phys. Rev. Lett. **121**, 204301 (2018).

[9] H. Li, A. Mekawy, and A. Alù, Beyond Chu's limit with Floquet impedance matching, Phys. Rev. Lett. **123**, 164102 (2019).

[10] H. Li and A. Alù, Temporal switching to extend the bandwidth of thin absorbers, Optica **8**, 24 (2021).

[11] V. Pacheco-Peña and N. Engheta, Antireflection temporal coatings, Optica **7**, 323 (2020).

[12] M. S. Mirmoosa, G. A. Ptitcyn, V. S. Asadchy, and S. A. Tretyakov, Time-varying reactive elements for extreme accumulation of electromagnetic energy, Phys. Rev. Appl. **11**, 014024 (2019).

[13] H. Li, H. Moussa, D. Sounas, and A. Alù, Parity-time symmetry based on time modulation, Phys. Rev. Appl. **14**, 031002(R) (2020).

[14] Z. Yu and S. Fan, Complete optical isolation created by indirect interband photonic transitions, Nat. Photon. **3**, 91 (2009).

[15] N. A. Estep, D. L. Sounas, J. Soric, and A. Alù, Magnetic-free non-reciprocity and isolation based on parametrically modulated coupled-resonator loops, Nat. Phys. **10**, 923 (2014).

[16] Z. Chen, Y. Peng, H. Li, J. Liu, Y. Ding, B. Liang, X.-F. Zhu, Y. Lu, J. Cheng, and A. Alù, Efficient nonreciprocal mode transitions in spatiotemporally modulated acoustic metamaterials, Sci. Adv. **7**, eabj1198 (2022).

[17] X. Wen, X. Zhu, A. Fan, W. Y. Tam, J. Zhu, H. W. Wu, F. Lemoult, M. Fink, and J. Li, Unidirectional amplification with acoustic non-Hermitian space−time varying metamaterial, Commun. Phys. **5**, 18 (2022).

[18] L. Lu, J. D. Joannopoulos, and M. Soljačić, Topological photonics, Nat. Photon. **8**, 821 (2014).

[19] T. Ozawa, H. M. Price, A. Amo, N. Goldman, M. Hafezi, L. Lu, M. C. Rechtsman, D. Schuster, J. Simon, O. Zilberberg, and I. Carusotto, Topological photonics, Rev. Mod. Phys. **91**, 015006 (2019).

[20] G. Ma, M. Xiao, and C. T. Chan, Topological phases in acoustic and mechanical systems, Nat. Rev. Phys. **1**, 281 (2019).

[21] W. Zhu, J. Gong, and R. W. Bomantara, Topological π modes and beyond, Sci. Bull. **67**, 2145 (2022).

[22] M. C. Rechtsman, J. M. Zeuner, Y. Plotnik, Y. Lumer, D. Podolsky, F. Dreisow, S. Nolte, M. Segev, and A. Szameit, Photonic Floquet topological insulators, Nature (London) **496**, 196 (2013).

[23] K. Fang, Z. Yu, and S. Fan, Realizing effective magnetic field for photons by controlling the phase of dynamic modulation, Nat. Photon. **6**, 782 (2012).

[24] R. Fleury, A. B. Khanikaev, and A. Alù, Floquet topological insulators for sound, Nat. Commun. **7**, 11744 (2016).

[25] A. Darabi, X. Ni, M. Leamy, and A. Alù, Reconfigurable Floquet elastodynamic topological insulator based on synthetic angular momentum bias, Sci. Adv. **6**, eaba8656 (2020).

[26] L. J. Maczewsky, J. M. Zeuner, S. Nolte, and A. Szameit, Observation of photonic anomalous Floquet topological insulators, Nat. Commun. **8**, 13756 (2017).

[27] Y.-G. Peng, Y. Li, Y.-X. Shen, Z.-G. Geng, J. Zhu, C.-W. Qiu, and X.-F. Zhu, Chirality-assisted three-dimensional acoustic Floquet lattices, Phys. Rev. Res. **1**, 033149 (2019).

[28] Y. Long and J. Ren, Floquet topological acoustic resonators and acoustic Thouless pumping, J. Acoust. Soc. Am. **146**, 742 (2019).

[29] Q. Cheng, Y. Pan, H. Wang, C. Zhang, D. Yu, A. Gover, H. Zhang, T. Li, L. Zhou, and S. Zhu, Observation of anomalous π modes in photonic Floquet engineering, Phys. Rev. Lett. **122**, 173901 (2019).

[30] S. Mukherjee, A. Spracklen, M. Valiente, E. Andersson, P. Öhberg, N. Goldman, and R. R. Thomson, Experimental observation of anomalous topological edge modes in a slowly driven photonic lattice, Nat. Commun. **8**, 13918 (2017).

[31] B. Wang, J. Quan, J. Han, X. Shen, H. Wu, and Y. Pan, Observation of Photonic Topological Floquet Time Crystals, Laser Photon Rev. **16**, 2100469 (2022).

[32] W. Zhu, H. Xue, J. Gong, Y. Chong, and B. Zhang, Time-periodic corner states from Floquet higher-order topology, Nat. Commun. **13**, 11 (2022).

[33] Z. Cheng, R. W. Bomantara, H. Xue, W. Zhu, J. Gong, and B. Zhang, Observation of $\pi/2$ modes in an acoustic Floquet system, Phys. Rev. Lett. **129**, 254301 (2022).

[34] O. Zilberberg, S. Huang, J. Guglielmon, M. Wang, K. P. Chen, Y. E. Kraus, and M. C. Rechtsman, Photonic topological boundary pumping as a probe of 4D quantum Hall physics, Nature (Lond.) **553**, 59 (2018).

[35] Z. Chen, Z. Chen, Z. Li, B. Liang, G. Ma, Y. Lu, and J. Cheng, Topological pumping in acoustic waveguide arrays with hopping modulation, New J. Phys. **24**, 013004 (2021).

[36] Q. Cheng, H. Wang, Y. Ke, T. Chen, Y. Yu, Y. S. Kivshar, C. Lee, and Y. Pan, Asymmetric topological pumping in nonparaxial photonics, Nat. Commun. **13**, 249 (2022).

[37] Z.-G. Chen, W. Tang, R.-Y. Zhang, Z. Chen, and G. Ma, Landau-Zener transition in the dynamic transfer of acoustic topological states, Phys. Rev. Lett. **126**, 054301 (2021).

[38] Y.-X. Shen, Y.-G. Peng, D.-G. Zhao, X.-C. Chen, J. Zhu, and X.-F. Zhu, One-way localized adiabatic passage in an acoustic system, Phys. Rev. Lett. **122**, 094501 (2019).

[39] Z.-G. Chen, R.-Y. Zhang, C. T. Chan, and G. Ma, Classical non-Abelian braiding of acoustic modes, Nat. Phys. **18**, 179 (2022).

[40] O. You, S. Liang, B. Xie, W. Gao, W. Ye, J. Zhu, and S. Zhang, Observation of non-Abelian Thouless pump, Phys. Rev. Lett. **128**, 244302 (2022).

[41] J. K. Asbóth, B. Tarasinski, and P. Delplace, Chiral symmetry and bulk-boundary correspondence in periodically driven one-dimensional systems, Phys. Rev. B **90**, 125143 (2014).

[42] V. Dal Lago, M. Atala, and L. E. F. Foa Torres, Floquet topological transitions in a driven one-dimensional topological insulator, Phys. Rev. A **92**, 023624 (2015).

[43] M. Fruchart, Complex classes of periodically driven topological lattice systems, Phys. Rev. B **93**, 115429 (2016).

[44] X. Ni, M. Li, M. Weiner, A. Alù, and A. B. Khanikaev, Demonstration of a quantized acoustic octupole topological insulator, Nat. Commun. **11**, 2108 (2020).

[45] Y. Qi, C. Qiu, M. Xiao, H. He, M. Ke, and Z. Liu, Acoustic realization of quadrupole topological insulators, Phys. Rev. Lett. **124**, 206601 (2020).

[46] H. Xue, Y. Ge, H.-X. Sun, Q. Wang, D. Jia, Y.-J. Guan, S.-Q. Yuan, Y. Chong, and B. Zhang, Observation of an acoustic octupole topological insulator, Nat. Commun. **11**, 2442 (2020).

[47] See Supplemental Material at http://link.aps.org/supplemental/10.1103/PhysRevB.109.L020302 for more details about the experimental setup and measurement, acoustic coupling with air tube or electric setups, experimental results of zero-energy mode, simulations of the Floquet π modes in waveguide systems and our dynamic lattice. It also contain Refs. [55,56].

[48] K. Ding, G. Ma, M. Xiao, Z. Q. Zhang, and C. T. Chan, Emergence, coalescence, and topological properties of multiple exceptional points and their experimental realization, Phys. Rev. X **6**, 021007 (2016).

[49] L. Zhang, Y. Yang, Y. Ge, Y.-J. Guan, Q. Chen, Q. Yan, F. Chen, R. Xi, Y. Li, D. Jia, S.-Q. Yuan, H.-X. Sun, H. Chen, and B. Zhang, Acoustic non-Hermitian skin effect from twisted winding topology, Nat. Commun. **12**, 6297 (2021).

[50] Q. Zhang, Y. Li, H. Sun, X. Liu, L. Zhao, X. Feng, X. Fan, and C. Qiu, Observation of acoustic non-Hermitian Bloch braids and associated topological phase transitions, Phys. Rev. Lett. **130**, 017201 (2023).

[51] M. Rodriguez-Vega and B. Seradjeh, Universal fluctuations of Floquet topological invariants at low frequencies, Phys. Rev. Lett. **121**, 036402 (2018).

[52] M. Lyubarov, Y. Lumer, A. Dikopoltsev, E. Lustig, Y. Sharabi, and M. Segev, Amplified emission and lasing in photonic time crystals, Science **377**, 425 (2022).

[53] T. Liu, J.-Y. Ou, K. F. MacDonald, and N. I. Zheludev, Photonic metamaterial analogue of a continuous time crystal, Nat. Phys. **19**, 986 (2023).

[54] H. Li, S. Yin, H. He, J. Xu, A. Alù, and B. Shapiro, Stationary charge radiation in anisotropic photonic time crystals, Phys. Rev. Lett. **130**, 093803 (2023).

[55] Z.-G. Chen, L. Wang, G. Zhang, and G. Ma, Chiral symmetry breaking of tight-binding models in coupled acoustic-cavity systems, Phys. Rev. Appl. **14**, 024023 (2020).

[56] J. K. Asbóth, L. Oroszlány, and A. Pályi, A short course on topological insulators, Lect. Notes Phys. **919**, 166 (2016).